J Solid State Electrochem (2008) 12:1101–1107
DOI 10.1007/s10008-007-0445-7

ORIGINAL PAPER

Pseudocapacitive behaviors of nanostructured manganese dioxide/carbon nanotubes composite electrodes in mild aqueous electrolytes: effects of electrolytes and current collectors

Yuqin Wang · Anbao Yuan · Xiuling Wang

Received: 23 July 2007 / Revised: 25 September 2007 / Accepted: 28 September 2007 / Published online: 23 October 2007

Abstract Nanostructured MnO_2/carbon nanotubes composite electrode material was prepared using the liquid-phase deposition reaction starting with potassium permanganate ($KMnO_4$) and manganese acetate ($Mn(Ac)_2{\cdot}4H_2O$) as the reactants and carbon nanotubes (CNTs) as the substrates. The structure and morphology of the material was characterized by X-ray diffraction, infrared spectroscopy, and transmission electron microscope techniques. The electrochemical properties of the nano-MnO_2/CNTs composite electrode in 1 M LiAc and 1 M $MgSO_4$ solutions and in 1 M RAc (R=Li, Na, and K)–1 M $MgSO_4$ mixed solutions, respectively, were studied. Experimental results demonstrated that the specific capacitance and rate discharge ability of the nano-MnO_2/CNTs composite electrode in 1 M LiAc–1 M $MgSO_4$ mixed solution is superior to that in 1 M LiAc or 1 M $MgSO_4$ solution. For the 1 M RAc (R=Li, Na, and K)–1 M $MgSO_4$ mixed electrolytes, the specific capacitance of the composite electrode was found to be in the following order: LiAc > NaAc > KAc.

Keywords Nano-MnO_2/CNTs composite electrode material · Pseudocapacitive behavior · Current collector · Mild aqueous mixed electrolyte

Introduction

Electrochemical supercapacitors are charge storage devices between traditional electrostatic capacitors and conventional secondary batteries [1], which have the characteristics of higher energy densities than the electrostatic capacitors and higher power densities than the secondary batteries, and attracted great attentions in the world. Based on charge storage mechanisms, supercapacitors can be divided into electric double layer capacitors (EDLCs) and redox pseudocapacitors. Compared to EDLC capacitance, the pseudocapacitance is much higher. For example, the specific capacitance of the amorphous hydrated $RuO_2{\cdot}nH_2O$ was reported to be as high as 720 F g^{-1} [2]. However, it is too expensive to be commercially accepted. Being similar to RuO_2, some comparatively inexpensive transition metal oxides, such as NiO [3], Co_3O_4 [4], etc., can also exhibit pseudocapacitance, and hence attracted attentions.

Since the first report on faradic pseudocapacive behaviors of nano-MnO_2 in mild aqueous KCl electrolyte by Lee and Goodenough in 1999 [5], nano-MnO_2 electrodes [6–16] and nano-MnO_2/activated carbon hybrid supercapacitors [17–19] became a hotspot in the scientific area of supercapacitors. Among various metal oxides, the nanostructured manganese dioxide has the advantages of high surface area, high specific capacitance, and wide charge/discharge potential range, resourceful, inexpensive, and environmental compatibility, being considered to be the most promising substitution electrode material for RuO_2. Carbon nanotubes (CNTs) are good conductive materials with EDLC capacitance. Hence, the nano-MnO_2/CNTs composite as an electrode material for supercapacitor applications attracted great attentions in recent years [19–27]. With regard to electrolyte for use in nano-MnO_2 capacitor, a variety of electrolytes have been tested and studied; majority are potassium or sodium sulfate, nitrate, and chloride aqueous solutions. It is well known that the nickel foam is usually used as an electrode current collector in nickel/metal hydride batteries because of its good

Y. Wang · A. Yuan (✉) · X. Wang
Department of Chemistry,
College of Sciences, Shanghai University,
Shanghai 200444, China
e-mail: abyuan@shu.edu.cn

stability in alkaline electrolytes. However, it can not be used in neutral aqueous electrolytes due to its oxidative corrosion upon electrode charging process. Hence, corrosion-resistive metals such as titanium, stainless steel, or noble metals (gold or platinum) are usually employed as current collectors, and these certainly increase the cost from the viewpoint of application. Compared with the two-dimensional titanium mesh or other noble metal mesh current collectors, the nickel foam current collector has the characteristic of three-dimensional porous structure with three-dimensional electrical conductive network, which can be expected to increase the utilization of electrode active material. Besides, the nickel foam current collector has the superiority of relatively lower cost with technical maturity. According to the literature [28], nano-MnO_2 electrode can exhibit a better supercapacitive property in aqueous $(NH_4)_2SO_4$ solution, but the foamed nickel current collector was found to be corrosive in this solution. The authors also found that addition of appropriate amount of $MgSO_4$ to the solution can inhibit the corrosion of the foamed nickel current collector.

In the present work, the nano-MnO_2/CNTs composite electrode material was prepared using the method described in literature [19], and the pseudocapacitive behaviors of the nano-MnO_2/CNTs composite electrode in 1 M LiAc and 1 M $MgSO_4$ solutions and in 1 M RAc (R=Li, Na, and K)–1 M $MgSO_4$ mixed solutions were investigated, respectively, using electrochemical methods. The titanium mesh and the nickel foam were respectively used as the current collectors for comparison.

Experimental

Preparation of nano-MnO_2/CNTs composite material and nano-MnO_2 material

Given amount of $KMnO_4$ and $Mn(Ac)_2{\cdot}4H_2O$ were dissolved respectively in distilled water to form solutions. Then, a given amount of CNTs (commercial product) were added to the $KMnO_4$ solution under stirring. Stirred for some time, the $Mn(Ac)_2$ solution was added to the above solution drop by drop, resulting in chemical reaction of $KMnO_4$ with $Mn(Ac)_2$ (mol ratio, 2:3). Reacting for 8 h under stirring, the product was washed with distilled water repeatedly and dried at 120 °C for 12 h. Thus, the nano-MnO_2/CNTs composite electrode material was obtained. The mass percent of CNTs in the final composite is about 10 wt%. In addition, pure nano-MnO_2 electrode material without CNTs addition was also prepared based on the above reaction of $KMnO_4$ with $MnAc_2$ for comparative study.

Characterization of nano-MnO_2/CNTs composite material

X-ray diffraction (XRD) analysis was performed on a Rigaku D/max–2000 X-ray diffractometer with CuK_α radiation (40 kV/250 mA; 2θ range, 10°~90°; scan rate, 0.02° S^{-1}). Infrared spectroscopic (IR) analysis was carried out using a Nicolet Avatar 370 Fourier transformation infrared (FT-IR) spectrometer (KBr pelleting, wave number range, 400~4,000 cm^{-1}). Transmission electron microscopy (TEM) observation was conducted on a JEOL JEM-200CX transmission electron microscope.

Preparation of nano-MnO_2/CNTs composite electrode and nano-MnO_2 electrode

Preparation of the nano-MnO_2/CNTs composite electrode The nano-MnO_2/CNTs composite material was mixed with acetylene black and polytetrafluoroethylene (PTFE) suspension to form slurry. The slurry was coated on to a foamed nickel or titanium mesh current collector (1× 1 cm^2), then dried at 70 °C and rolled to a sheet of about 0.6 mm thickness. The loading mass of nano-MnO_2/CNTs in the composite electrode is about 0.04 g. When foamed nickel was used as a current collector, the mass ratio of nano-MnO_2–CNTs/acetylene black/PTFE=80:15:5; When titanium mesh was used as a current collector, the mass ratio is 75:20:5. This is because the current-collection effect of the titanium mesh is poor than that of the foamed nickel, and hence, more acetylene black conductor should be added.

Preparation of the nano-MnO_2 electrode Foamed nickel was used as a current collector, and the mass ratio of nano-MnO_2/acetylene black/PTFE=80:15:5. The others are the same as the above procedure.

Electrochemical testing

Electrochemical tests were conducted using a three-electrode system. The nano-MnO_2/CNTs composite electrode or the nano-MnO_2 electrode served as the working electrode. An activated carbon electrode and a saturated calomel electrode (SCE) were served as the counter electrode and the reference electrode, respectively. About 1 M LiAc or 1 M $MgSO_4$ solution or 1 M RAc (R=Li, Na, and K)–1 M $MgSO_4$ mixed solution was used as the electrolyte. Cyclic voltammetry and AC impedance measurements were carried out on a Solartron 1287 electrochemical interface coupled with a 1255B frequency response analyzer. Galvanostatic charge/discharge tests were performed on a LAND auto-cycler (China). All of the work was done at room temperature.

Results and discussion

Structural characterization and morphological observation of nano-MnO_2/CNTs composite material

Figure 1 shows the XRD pattern of the nano-MnO_2/CNTs composite. The peak occurred at 2θ around 26° should be indexed to the characteristic diffraction peak of CNTs [27], while the peaks around 11, 37, 66, and 78° can be indexed to birnessite-type MnO_2 (JCPDS 42–1317), which is similar to the report in literature [27]. Hence, the manganese oxide in the composite should be attributed to the potassium manganese oxide hydrate (birnessite δ–$MnO_2{\cdot}nH_2O$) with 2D layered structure, which incorporates K^+ ions and H_2O molecules in the interlayer. The incorporation of K^+ ions should come from the reactant $KMnO_4$. In addition, it can be seen from the diffraction pattern that the crystallinity of the deposited MnO_2 is not very high but exhibiting partial amorphization.

Figure 2 shows the infrared spectrum (IR) of the nano-MnO_2/CNTs composite. Several absorption bands can be observed at 3,360, 1,620, 1,540, 1,400, 1,340, 1,020, and 535 cm^{-1}, respectively. The 3,360 cm^{-1} band should be attributed to the O–H stretching vibration, and the 1,620, 1,540, 1,400, 1,340, and 1,020 cm^{-1} bands are usually attributed to the O–H bending vibrations combined with Mn atoms. The 535 cm^{-1} band should be ascribed to the Mn–O vibrations in MnO_6 octahedra [29]. The IR result suggests the presence of some constitutional water incorporated in the MnO_2 structure. This result further confirms that the manganese oxide in the composite is hydrous MnO_2.

Figure 3 displays the TEM image of the MnO_2/CNTs composite with a magnification factor of 100,000. It can be seen from Fig. 3 that the CNTs are cross-entwisted with the tube-diameter ranging from about 20 to 40 nm. A majority of the MnO_2 particles with a size ranging from about 10 to 100 nm are adhered to the CNTs, with a distribution from dense deposition in somewhere to non-dense deposition in elsewhere.

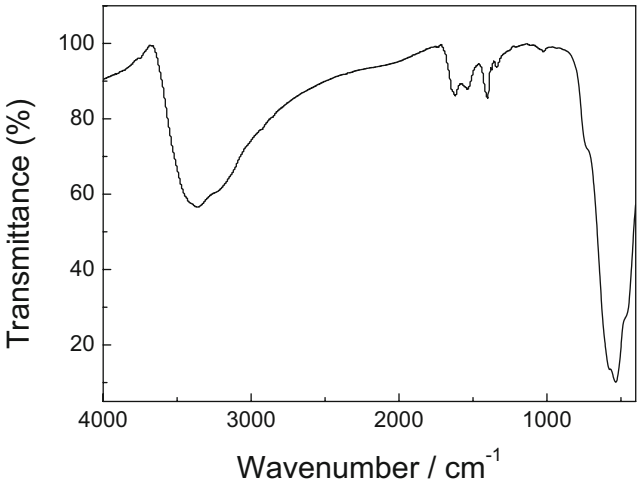

Fig. 2 FT-IR spectrum of the nano-MnO_2/CNTs composite

Study of pseudocapacitive behaviors

Influence of carbon nanotubes and acetylene black on specific discharge capacitance of nano-MnO_2 electrode

Specific discharge capacitance of the nano-MnO_2 electrodes with different compositions (electrodes A, B, and C) at various charge/discharge rates are listed in Table 1, where the foamed nickel was used as the current collector and the 1 M LiAc–1 M $MgSO_4$ mixed solution as the electrolyte. The electrodes were charged and discharged in the operating potential range 0~1.1 V (vs SCE) with the charge/discharge rates at 25, 50, and 100 mA g^{-1},

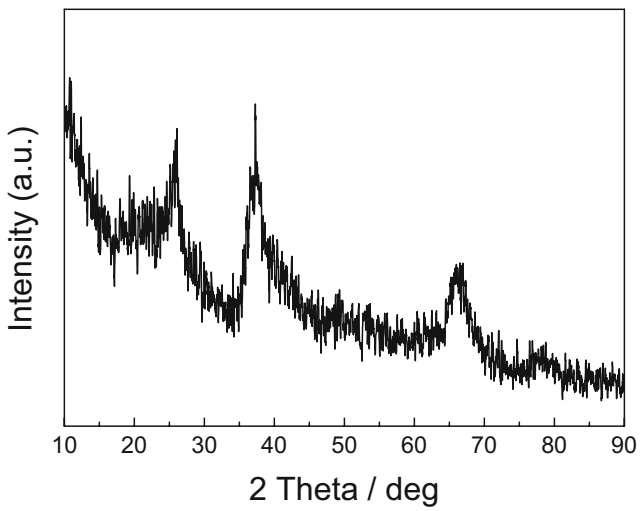

Fig. 1 XRD pattern of the nano-MnO_2/CNTs composite

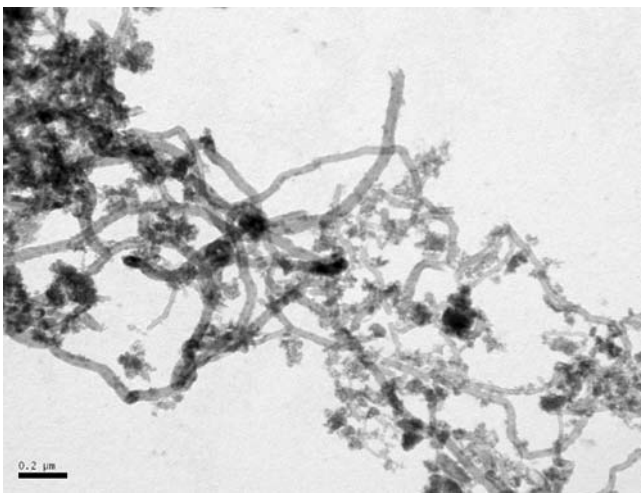

Fig. 3 TEM image of the nano-MnO_2/CNTs composite

Table 1 Specific discharge capacitance of the nano-MnO_2 electrodes with different compositions at different charge/discharge rates

Electrode	Specific discharge capacitance ($F \cdot g^{-1}$)		
	25 (mA g^{-1})	50 (mA g^{-1})	100 (mA g^{-1})
A (95 wt% nano-MnO_2/CNTs composite + 5 wt% PTFE)	98.5	91.4	54.9
B (80 wt% nano-MnO_2 + 15 wt% acetylene black + 5 wt% PTFE)	195.7	64.1	33.1
C (80 wt% nano-MnO_2/CNTs composite + 15 wt% acetylene black + 5 wt% PTFE)	204.8	112.3	94.0

respectively. The specific capacitance date are calculated according to the formula $C_s = (It)/(m\Delta V)$, where C_s is the specific discharge capacitance, I the discharge current, t the discharge time, ΔV the discharge potential range, and m the active material mass of the electrode (including the mass of nano-MnO_2 and CNTs, but not including the mass of acetylene black and PTFE). Comparing the specific capacitance data for electrodes A and B, we know that the specific capacitance of the electrode containing CNTs but not containing acetylene black (electrode A) at 25 mA g^{-1} is only 98.5 F g^{-1}, while the specific capacitance of the electrode containing acetylene black but not containing CNTs (electrode B) can reach 195.7 F g^{-1} at the same current rate. However, when the current rate increased to 50 mA g^{-1} or higher, the specific capacitance of the electrode B is lower than that of the electrode A. Among the three electrodes, the specific capacitance of the electrode containing CNTs and acetylene black (electrode C) is the highest, especially at higher rates. It can be concluded from this result that acetylene black conductor has a very favorable influence on the specific capacitance at a lower current rate, and the CNTs has a positive effect on the specific capacitance at a higher rate. Simultaneously addition of CNTs and acetylene black can obviously improve the charge/discharge performance of the nano-MnO_2 electrode. The different effects of CNTs and acetylene black may be explained as follows: The added acetylene black can form a "macroscopic" conductive network, providing good electronic conduction paths between the active material particles and between the active material particles and the current collector. Under the condition of a lower current rate, this effect caused by the acetylene black is more obvious, while under the condition of a higher current rate, this effect seems insufficient, and on the contrary, the CNTs then take effect principally. This is because the nano-MnO_2 was directly deposited on the CNTs that act as "microscopic" conductors.

Cyclic voltammetry

We found from experiments that, in mild aqueous electrolytes, corrosion can take place on foamed nickel current collector but not on titanium mesh current collector. However, addition of appropriate amount of $MgSO_4$ to a mild electrolyte can inhibit the corrosion of foamed nickel current collector. Hence, in this study, as long as the foamed nickel was used as a current collector, then $MgSO_4$ was added to the electrolyte. However, the anti-corrosion mechanism of $MgSO_4$ is not clear by now. Figure 4 shows the cyclic voltammograms (CVs) of the nano-MnO_2/CNTs composite electrodes with different current collectors (Ti mesh or Ni foam) in different electrolytes (scan rate, 1 mV s^{-1}). It can be seen that when the Ti mesh is used as a collector, a couple of redox peaks can be observed for the electrode in 1 M LiAc solution. The anodic and cathodic peaks occur at about 0.9 and 0.6 V, respectively. Being different from the case in 1 M LiAc solution, the CV of the electrode in 1 M $MgSO_4$ solution is similar to a rectangle approximately, but there are two specialties: (1) when positively scanned to about 1 V, the oxygen starts to evolved, and an obvious peak can be observed in the CV; (2) when negatively scanned to ca. 0.3 V, an increasing cathodic current response can be observed, and this can be attributed to the irreversible transformation from Mn(IV) to Mn(II) [22], and accordingly, an oxidation peak can also be observed at the potential around 0.35 V. From the point of view of thermodynamics, the equilibrium potential of the transformation from Mn(IV) to Mn(II) decreases with pH increasing [22]. At the temperature of 25 °C, the solubility product constant for $Mg(OH)_2$ is 1.8×10^{-11}, and the

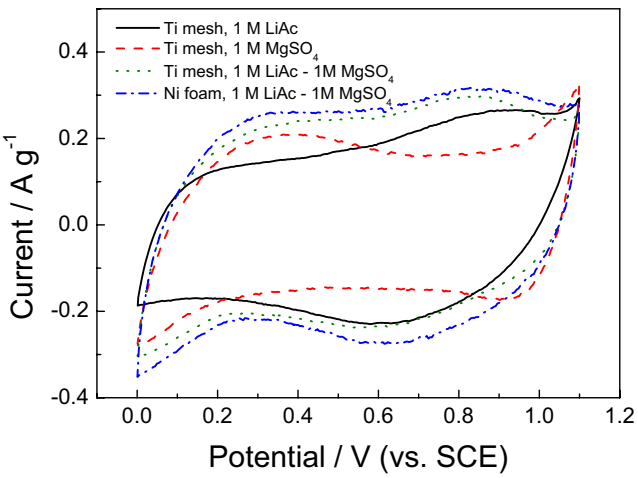

Fig. 4 Cyclic voltammograms of the nano-MnO_2/CNTs composite electrodes with different current collectors in different electrolytes

dissociation constant for HAc is 1.754×10^{-5}. Due to the hydrolysis caused by Ac^- or Mg^{2+} in aqueous solution, the pH for 1 M LiAc solution is higher than the pH for 1 M $MgSO_4$ solution, and hence, the reduction potential for Mn (IV) to Mn(II) transformation in 1 M $MgSO_4$ is higher than that in 1 M LiAc. Judging from the areas under the CV profiles, the specific capacitance of the electrode in 1 M LiAc solution is higher than that in 1 M $MgSO_4$ solution, and this can be attributed to the faradic pseudocapacitance contribution produced by the redox reaction around 0.75 V in 1 M LiAc solution. In 1 M LiAc–1 M $MgSO_4$ mixed solution, the CV has the combined characteristics of the two, i.e., two couples of redox peaks can be observed in the higher and the lower potential regions respectively. In addition, the conductivity of the mixed solution is higher than that of the two single solutions. Hence, the current response (or specific capacitance) of the electrode in the mixed solution is higher than that of the two electrodes in the single solutions. In the same electrolyte (1 M LiAc–1 M $MgSO_4$), the current response of the electrode with the Ni foam current collector is higher than that with the Ti mesh current collector, i.e., a higher specific capacitance can be obtained in the former case. This is because using the nickel foam current collector with a three-dimensional conductive network can improve the conductivity (see Fig. 6) or current-collection effect of the electrode, and hence increases the active material utilization of the electrode.

Figure 5 shows the CVs of the nano-MnO_2/CNTs composite electrodes with the foamed nickel current collector in 1 M LiAc–1 M $MgSO_4$, 1 M NaAc–1 M $MgSO_4$, and 1 M KAc–1 M $MgSO_4$ mixed electrolytes, respectively. It can be seen that the characteristics of the CVs are principally alike. However, the current response of the electrode in 1 M LiAc–1 M $MgSO_4$ electrolyte is

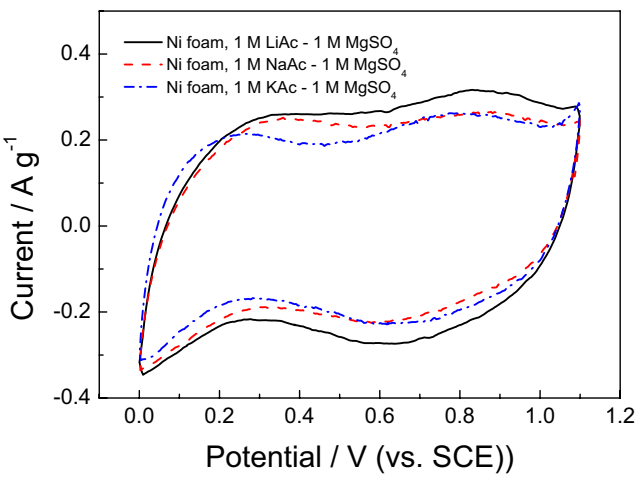

Fig. 5 Cyclic voltammograms of the nano-MnO_2/CNTs composite electrodes with the foamed nickel current collector in 1 M LiAc–1 M $MgSO_4$, 1 M NaAc–1 M $MgSO_4$, and 1 M KAc–1 M $MgSO_4$ mixed electrolytes, respectively

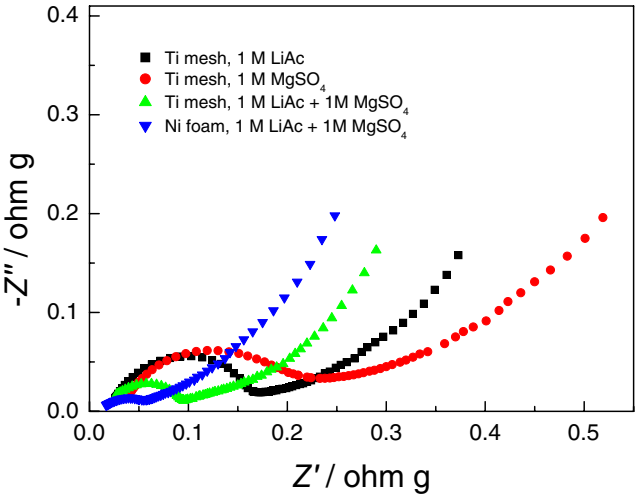

Fig. 6 Nyquist plots of AC impedance of the nano-MnO_2/CNTs composite electrodes with different current collectors in different electrolytes

obviously higher than the other two, suggesting a higher specific capacitance being reached in this electrolyte. Although there have been several studies dealing with the supercapacitive mechanism of MnO_2 electrode in mild aqueous electrolytes [5, 6, 14, 16, 30], the exact mechanism still remains unclear up to now. The reasons may exist in two aspects: First, the study of supercapacitive mechanism is difficult and complicated and second, supercapacitive mechanism may be associated with the structure and preparation of the MnO_2 electrode material and the kind, concentration, and pH of the electrolyte. According to the recent published papers [14, 16], the pseudocapacitance of the MnO_2 electrode in mild aqueous electrolytes appears to be associated with the intercalation/deintercalation reaction of protons and other available cations in MnO_2 solid. The redox reaction includes the charge transfer process at the electrode/electrolyte interface and the diffusion process in solid. Owing to the slow diffusion process in solid, the reaction is usually limited at the surface and/or subsurface of the electrode active material at a higher current density.

In the present work, the capacitance of the nano-MnO_2/CNTs composite electrode is suggested to be mainly the pseudocapacitance contribution from the redox reaction of the nano-MnO_2. Of course, there is also partial contribution from the double layer charging. The redox reaction can be viewed as H_3O^+ and alkali cations R^+ (R^+=Li^+, Na^+, and K^+) insertion/deinsertion in MnO_2 solid, accompanied by the charge transfer process at the electrode/electrolyte interface with variation of Mn valence state. The charge-storage reaction can be summarized as [14]:

$$\mathrm{Mn(IV)O_2}\cdot n\mathrm{H_2O}+\delta\mathrm{e}^-+\delta(1-f)\mathrm{H_3O}^+ +\delta f\mathrm{M}^+ \rightleftharpoons (\mathrm{H_3O})_{\delta(1-f)}\mathrm{M}_{\delta f}\left[\mathrm{Mn(III)}_{\delta}\mathrm{Mn(IV)}_{1-\delta}\right]\mathrm{O_2}\cdot n\mathrm{H_2O}$$

where M^+ is the alkali cation. We know that, in crystals, the approximate effective ionic radii of the cations Mg^{2+}, Li^+, Na^+, and K^+ are 0.66, 0.68, 0.97, and 1.33 Å respectively, while in aqueous solutions, the approximate effective ionic radii of the cations (i.e., the hydrated ionic radii) are 8, 6, 4, and 3 Å, respectively. In aqueous electrolytes, protons and other available cations have the possibility of insertion/abstraction in MnO_2 electrode, depending on the conditions. The pseudocapacitive charge-storage reaction of a fine-grained ε-$MnO_2{\cdot}nH_2O$ electrode in the aqueous alkali-chloride solutions was investigated in literature [14]. The results indicated that H_3O^+ plays the predominant (>60%) role in pseudocapacitance. As to which cation(s) can contribute and how much contributions, two energy factors would be considered. First, the increase in free energy caused by lattices expansion would favor insertion of smaller cations. Second, the increase of free energy by removal of water molecules from the solvated cation would favor large cations. The extent of insertion of either H_3O^+ or alkali cations would result from the balance between these two opposing factors. The redox peaks appearing around 0.75 V in Fig. 5 in the present work should be attributed to Li^+, Na^+, and K^+ insertion/abstraction in the MnO_2 electrode, respectively. This phenomenon is similar to the observation in literature [15], where a pair of redox peaks was observed in the CV for a birnessite δ-MnO_2 electrode in 0.1 M K_2SO_4 solution. It can be seen from Fig. 5 that, with radius of the alkali cations increasing, the peak current decreases. This suggests that with radius increasing, the insertion/abstraction reaction becomes difficult. However, no redox peaks could be observed for the electrode in 1 M $MgSO_4$ solution (see Fig. 4), suggesting no insertion/abstraction of Mg^{2+} ions in MnO_2 solid.

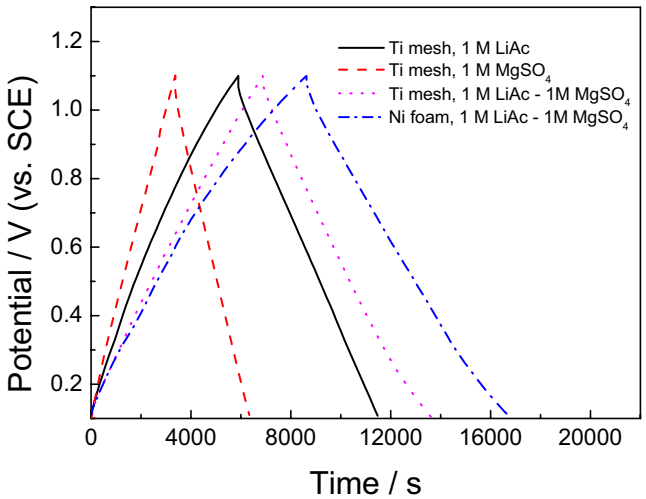

Fig. 7 Galvanostatic charge/discharge profiles of the nano-MnO_2/CNTs composite electrodes with different current collectors in different electrolytes at a current rate of 25 mA g^{-1}

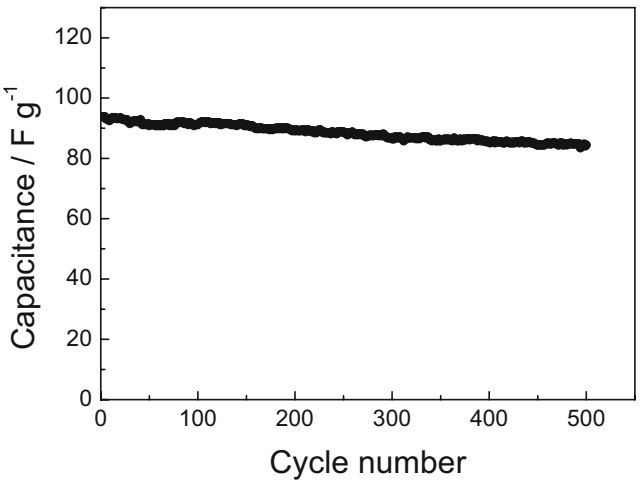

Fig. 8 Charge/discharge cycle life of the nano-MnO_2/CNTs composite electrode with the foamed nickel current collector in 1 M LiAc–1 M $MgSO_4$ electrolyte at a current rate of 100 mA g^{-1}

Correspondingly, the specific capacitance of the electrode is relatively lower. This is likely related to the bigger radius of hydrated Mg^{2+} ions. Before intercalation, the surrounding water molecules should be removed, and this process is difficult due to the high activation energy.

AC impedance

Figure 6 displays the Nyquist plots of AC impedance of the nano-MnO_2/CNTs composite electrodes with different current collectors in different electrolytes (frequency range, 10^5~10^{-2} Hz). It can be seen that all the impedances consist of an arc and a line. The arc at higher frequency region should be attributed to the charge transfer process coupled with double layer charging, and the line at lower frequency region should be ascribed to the solid diffusion in the MnO_2 electrode. A trend of increasing slope of the line can be observed at the lower frequency region, exhibiting a capacitive nature that is the typical characteristic of porous electrodes. Comparing these impedance spectra, we know that the electrolyte and current collector have obvious effects on the impedance behavior of the nano-MnO_2/CNTs composite electrode. When Ti mesh is used as a current collector, the charge transfer resistance for using different electrolytes follows the order: 1 M $MgSO_4$>1 M LiAc> 1 M LiAc–1 M $MgSO_4$. This result is consistent with the CV result in Fig. 4. Comparing the ohmic resistance, charge transfer resistance and diffusion impedance, the ohmic resistance is relatively lower, and the electrode kinetics is co-controlled by the charge transfer process at the electrode/electrolyte interface and the diffusion process in solid. With the charge transfer resistance decreasing, the electrode process is gradually converted to being governed by the solid diffusion process.

Galvanostatic charge/discharge

Figure 7 shows the galvanostatic charge/discharge profiles of the nano-MnO_2/CNTs composite electrodes with different current collectors in different electrolytes at a current rate of 25 mA g^{-1}. It can be seen from Fig. 7 that, in 1 M $MgSO_4$ electrolyte, the charge and the discharge profiles of the electrode are symmetrical, and a linear relationship between potential and time can be observed. For the electrodes in other three electrolytes, the charge profiles are curved somewhat at the later stage of charging process, indicating a faradic pseudocapacitive characteristic. This result is associated with the oxidation peak occurring in Fig. 4 at this potential range. The variation of discharge potential with time is almost linear. However, for the electrode in 1 M LiAc–1 M $MgSO_4$ solution, the reduction rate of discharge potential decreased when the potential is below approximately 0.3 V. This result is consistent with the observed increasing of cathodic current response when the potential is below 0.3 V (see Fig. 4). In addition, at the moment of current reversing (from charging to discharging), the potential drop (caused by polarization) for the electrodes in different electrolytes follows the order: 1 M $MgSO_4$>1 M LiAc>1 M LiAc–1 M $MgSO_4$>1 M LiAc–1 M $MgSO_4$ (Ni foam current collector), and this result is consistent with the AC impedance result in Fig. 6. According to the above order and based on the formula, $C_s = (It_d)/(m\Delta V)$, the average specific discharge capacitances of the electrodes are calculated to be 98.6, 162.4, 190.8, and 204.8 F g^{-1}, respectively. The order of specific capacitance is consistent with the CV result in Fig. 4.

Figure 8 presents the charge/discharge cycle life of the nano-MnO_2/CNTs composite electrode with foamed nickel scurrent collector in 1 M LiAc–1 M $MgSO_4$ electrolyte at a current rate of 100 mA g^{-1}. The electrode was charge/discharge cycled in the operating potential of 0~1.1 V (SCE). The initial specific discharge capacitance is 93.9 F g^{-1}, and the specific discharge capacitance at the 400th cycle and the 500th cycle are 85.5 and 84.5 F g^{-1}, respectively. That is to say, from the 400th cycle, the reduction of specific capacitance with cycle number becomes lower. The capacitance retention is 90% after 500 cycles, indicating a good charge/discharge cyclic stability.

Conclusions

The nanostructured MnO_2/CNTs composite electrode material was prepared starting with $KMnO_4$, $Mn(Ac)_2{\cdot}4H_2O$, and CNTs raw materials. XRD, IR, and TEM results demonstrated that in the MnO_2/CNTs composite, most of the MnO_2 are adhered to the CNTs and the deposited MnO_2 is potassium manganese oxide hydrate (birnessite δ-$MnO_2{\cdot}nH_2O$). The electrochemical properties of the nano-MnO_2/CNTs composite electrode in 1 M LiAc and 1 M $MgSO_4$ solutions and in 1 M RAc (R=Li, Na, and K)–1 M $MgSO_4$ mixed solutions were studied by cyclic voltammetry, AC impedance, and galvanostatic charge/discharge methods. The results showed that the specific capacitance and rate discharge ability of the nano-MnO_2/CNTs composite electrode in 1 M LiAc–1 M $MgSO_4$ mixed solution is superior to that in 1 M LiAc or 1 M $MgSO_4$ solution. The current-collection effect of the foamed nickel is superior to that of the titanium mesh. For the 1 M RAc (R=Li, Na, and K)–1 M $MgSO_4$ mixed electrolytes, the specific capacitance of the composite electrode was found to be in the following order: LiAc > NaAc> KAc.

References

1. Conway BE (1991) J Electrochem Soc 138:1539
2. Zheng JP, Cygan PJ, Jow TR (1995) J Electrochem Soc 142:2699
3. Nam KW, Yoon WS, Kim KB (2002) Electrochim Acta 47:3201
4. Srinivasan V, Weidner JW (2002) J Power Sources 108:15
5. Lee HY, Goodenough JB (1999) J Solid State Chem 144:220
6. Pang SC, Anderson MA, Chapman TW (2000) J Electrochem Soc 147:444
7. Toupin M, Brousse T, Bélanger D (2002) Chem Mater 14:3946
8. Reddy RN, Reddy RG (2003) J Power Sources 124:330
9. Prasad KR, Miura N (2004) J Power Sources 135:354
10. Chen YS, Hu CC, Wu YT (2004) J Solid State Electrochem 8:467
11. Subramanian V, Zhu HW, Vajtai R, Ajayan PM, Wei BQ (2005) J Phys Chem B 109:20207
12. Broughton JN, Brett MJ (2005) Electrochim Acta 50:4814
13. Nam KW, Kim KB (2006) J Electrochem Soc 153:A81
14. Kuo SL, Wu NL (2006) J Electrochem Soc 153:A1317
15. Brousse T, Toupin M, Dugas R, Athouël L, Crosnier O, Bélanger D (2006) J Electrochem Soc 153:A2171
16. Chun SE, Pyun SI, Lee GJ (2006) Electrochim Acta 51:6479
17. Hong MS, Lee SH, Kim SW (2002) Electrochem Solid-State Lett 5:A227
18. Brousse T, Toupin M, Bélanger D (2004) J Electrochem Soc 151: A614
19. Khomenko V, Raymundo-Piñero E, Béguin F (2006) J Power Sources 153:183
20. Wu YT, Hu CC (2004) J Electrochem Soc 151:A2060
21. Zhou YK, He BL, Zhang FB, Li HL (2004) J Solid State Electrochem 8:482
22. Raymundo-Piñero E, Khomenko V, Frackowiak E, Béguin F (2005) J Electrochem Soc 152:A229
23. Lee CY, Tsai HM, Chuang HJ, Li SY, Lin P, Tseng TY (2005) J Electrochem Soc 152:A716
24. Wang GX, Zhang BL, Yu ZL, Qu MZ (2005) Solid State Ionics 176:1169
25. Subramanian V, Zhu HW, Wei BQ (2006) Electrochem Commun 8:827
26. Fan Z, Chen JH, Wang MY, Cui KZ, Zhou HH, Kuang YF (2006) Diam Relat Mater 15:1478
27. Ma SB, Ahn KY, Lee ES, Oh KH, Kim KB (2007) Carbon 45:375
28. Zhang ML, Yang C, Chen Y, Xue Y (2004) Chin J Power Sources 28:626
29. Ananth M V, Pethkar S, Dakshinamurthi K (1998) J Power Sources 75:278
30. Toupin M, Brousse T, Bélanger D (2004) Chem Mater 16:3184